

**Relative stability and local curvature analysis in carbon nanotori**Chern Chuang,<sup>1</sup> Jie Guan,<sup>2</sup> David Witalka,<sup>2</sup> Zhen Zhu,<sup>2</sup> Bih-Yaw Jin,<sup>3</sup> and David Tománek<sup>2,\*</sup><sup>1</sup>*Department of Chemistry, Massachusetts Institute of Technology, Cambridge, Massachusetts 02139, USA*<sup>2</sup>*Physics and Astronomy Department, Michigan State University, East Lansing, Michigan 48824, USA*<sup>3</sup>*Department of Chemistry and Center for Emerging Material and Advanced Devices, National Taiwan University, Taipei 10617, Taiwan*

(Received 13 March 2015; revised manuscript received 14 April 2015; published 29 April 2015)

We introduce a concise formalism to characterize nanometer-sized tori based on carbon nanotubes and to determine their stability by combining *ab initio* density functional calculations with a continuum elasticity theory approach that requires only shape information. We find that the high strain energy in nanotori containing only hexagonal rings is significantly reduced in nanotori containing also other polygons. Our approach allows to determine local curvature and link it to local strain energy, which is correlated with local stability and chemical reactivity.

DOI: [10.1103/PhysRevB.91.165433](https://doi.org/10.1103/PhysRevB.91.165433)

PACS number(s): 61.48.De, 68.55.ap, 61.46.–w, 81.05.ub

**I. INTRODUCTION**

The past three decades witnessed an unprecedented progress in the synthesis and use of nanostructures consisting of elemental carbon, ranging from fullerenes to carbon nanotubes and graphene [1–4]. Due to the stiffness of the  $\sigma$  bonding network and the delocalization of the  $\pi$  electrons in these systems, the structure-property relationships are highly nontrivial, as presence of local atomic defects is known to affect physical properties on the mesoscopic length scale [5]. In this regard, owing to their peculiar geometry and topology [6], carbon nanotori based on single-wall carbon nanotubes serve as an excellent test ground for studying such effects. To name just a few, reversible elastic deformation of carbon nanotori has been predicted [7] and experimentally identified [8], implying potential application in force-sensing devices. Gigantic paramagnetic response [9], persistent currents [10–12], and even molecular anapole moments [13] have been predicted for specific nanotorus geometries. Also, the intricate shape of carbon nanotori can be exploited in the context of host-guest chemistry and physics; for example, megahertz oscillations of a nanotorus mounted on a nanotube [14] and metal-encapsulated nanotori with net magnetic moment [15] have been predicted. A crucial prerequisite to realize these interesting physical properties is to establish, to what degree the postulated toroidal nanostructures are stable mechanically and thermally.

Here, we study the stability of carbon nanotori formed conceptually by bending a finite-length single-wall carbon nanotube (CNT) and connecting its ends seamlessly. Such a nanotorus can then be characterized by the chiral index [16]  $(n, m)$  of the nanotube and number of primitive unit cells along the perimeter. We will refer to this family of nanotori, which contain only hexagonal rings, as *polyhex* nanotori. It is known that presence of nonhexagonal rings, such as 5–7 pairs, induces a bend in a straight nanotube. In the following, we will refer to the family of nanotori that contain also nonhexagonal rings as *polygonal* nanotori. We will demonstrate that a continuum elasticity theory approach [17], which requires only shape information, is capable of estimating not only the global

stability, but also local strain with a precision approaching that of *ab initio* density functional calculations at a small fraction of the computational cost.

Our manuscript is organized as follows. In the next section, we outline the computational techniques used in our study. Next, we summarize the characteristics of different nanotori families. Then, we analyze and obtain analytical expressions for the in-plane and out-of-plane contributions to the elastic energy of polyhex nanotori. In the following section, we will present a general overview of the elastic energy for polygonal nanotori. Next, we will discuss the distributions of curvature and elastic energy on polygonal nanotori, and correlate them with the relative positions of the nonhexagonal rings in the systems. This is followed by the asymptotic analysis of three families of polygonal nanotori with varying shape parameters, including changing rotational symmetry, the lateral torus size normal to the axis and the torus height along the axis.

**II. COMPUTATIONAL TECHNIQUES**

Our main computational approach is based on continuum elasticity theory, which proved useful in evaluating the strain energy in fullerenes, nanotubes, and schwarzites with respect to a planar graphene monolayer and corresponding stability differences [17].

In systems with no frustration, where areas of Voronoi polygons associated with individual atoms are at the optimum value, the in-plane strain energy is very small. This proved to be the case in carbon nanotubes [17] and we expect it to hold also in the related nanotori. Neglecting the in-plane component of strain, the stability of nanotori could be analyzed in the inextensional limit of the mechanical theory of a membrane [18], where the elastic energy is dominated by its out-of-plane component.

The out-of-plane strain or curvature energy of a given closed membrane can be expressed as

$$\Delta E_c = D \int_S dA [2k^2 - (1 - \alpha)G], \quad (1)$$

where  $D$  is the flexural rigidity,  $\alpha$  is the Poisson ratio,  $k$  is the local mean curvature,  $G$  is the local Gaussian curvature, and the integration is carried out over the surface  $S$  of the membrane. If instead of the general shape we know the

\*tomanek@pa.msu.edu

precise atomic locations from either diffraction experiments or *ab initio* calculations, we can rather use the discretized version of Eq. (1),

$$\Delta E_c \approx A_0 D \sum_i [2k_i^2 - (1 - \alpha)G_i]. \quad (2)$$

Here,  $A_0$  is the area per atom,  $k_i$  is the local mean curvature, and  $G_i$  is the local Gaussian curvature at atom site  $i$ . The summation covers all atoms of the torus. For structures comprising of more than one element, the quantity  $A_0$  may vary and needs to be taken inside of the summation. Alongside with this expression, accurate ways to estimate  $k_i$  and  $G_i$  based on the *local geometry* in the vicinity of site  $i$  have been proposed recently [17], which have been validated by *ab initio* density functional calculations. Even though this method relies on the knowledge of the molecular geometry, it has been shown that even inexpensive classical force fields serve the purpose of structure optimization surprisingly well when compared against state-of-the-art *ab initio* calculations for a wide range of graphitic structures [17,19].

The total in-plane strain energy can be estimated in the continuum model from an integral over the entire surface area  $A$ ,

$$\Delta E_s = \oint_A \epsilon(\sigma) dA, \quad (3)$$

where  $\epsilon(\sigma)$  is the energy cost per area subject to strain  $\sigma$ . For specific, small strains,  $\epsilon(\sigma)$  may be presented as a harmonic function of the strain  $\sigma$ , with the proper coefficient taken either from experimental data or from *ab initio* calculations.

Selected results based on continuum elasticity theory are validated by *ab initio* calculations in the framework of density functional theory (DFT), as implemented in the SIESTA code [20]. We use the local density approximation [21,22] to describe exchange and correlation in the system, norm-conserving Troullier-Martins pseudopotentials [23], and a double- $\zeta$  basis including polarization orbitals. In the reference system, we sample the 2D Brillouin zone of graphene by  $16 \times 16$   $k$  points [24]. The small Brillouin zones of isolated nanotori are sampled by only 1  $k$  point. We use a mesh cutoff energy of 180 Ry to determine the self-consistent charge density, which provides precision in total energy of  $\lesssim 2$  meV/atom. All geometries are optimized using the conjugate gradient method [25], until none of the residual Hellmann-Feynman forces exceeds  $10^{-2}$  eV/Å.

### III. NANOTORUS CHARACTERISTICS

Due to the extreme flexural stiffness of straight CNTs [26,27], it is expected that the number of carbon atoms of a stable polyhex nanotorus should be at least on the order of  $10^5$ . An example of a polyhex nanotorus containing 400 carbon atoms is shown in Fig. 1(a). From the two shaded hexagons located in the inner and the outer rims of the nanotorus, it is obvious that the in-plane strain energy is inversely proportional to the size of the nanotori. This will be addressed in detail in the following section.

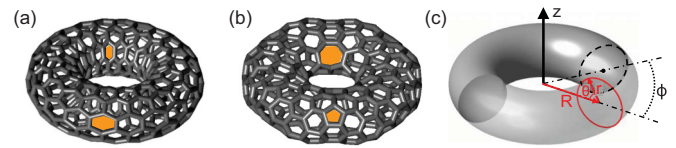


FIG. 1. (Color online) Atomic structure of (a) a polyhex nanotorus with only hexagons and (b) a polygonal nanotorus containing nonhexagonal rings. (c) A model of a perfect torus with major radius  $R$  and minor radius  $r$ .  $\theta$  is the longitudinal angle and  $\phi$  is the azimuthal angle. The yellow shading in (a) and (b) indicates specific polygons in the nanotori.

In contrast to polyhex nanotori, there has been considerable effort in describing the second family of polygonal nanotori, which also contain nonhexagonal rings. Due to the requirement of trivalency of  $sp^2$  carbon atoms and the Euler's theorem, the number of nonhexagonal rings on a general closed surface is constrained by

$$\sum_{m>2} (6 - m)N_m = 6\chi, \quad (4)$$

where  $N_m$  is the number of the  $m$ -gonal rings and  $\chi$  is the Euler characteristic of the closed surface in question. For a torus, we have  $\chi = 0$ . Thus, if we restrict ourselves to polygonal nanotori having only pentagons, hexagons, and heptagons, the number of pentagons,  $N_5$ , must equal that of heptagons,  $N_7$ . Apart from this simple equation, there are many more combinatorial and geometrical constraints for a stable polygonal carbon nanotorus to exist [28]. The polygonal nanotori covered in this study are restricted to those of high symmetry ( $D_{nd}$  or  $D_{nh}$  point group) and a smaller number of atoms ( $< 60$  atoms per rotational unit cell). One such polygonal nanotorus is shown in Fig. 1(b), a representative pentagon on the outer and a heptagon on the inner side of the nanotorus are highlighted. As suggested before, the existence of these nonhexagonal rings induces natural bending and thus drastically reduces the in-plane strain energy.

### IV. ELASTIC ENERGY IN NANOTORI

As suggested above, the elastic energy within carbon nanotori can be divided into two parts, namely the in-plane and the out-of-plane strain energy. The in-plane strain originates from an uneven distribution of atomic area densities as compared to graphene at equilibrium. This is most obvious in polyhex nanotori, where hexagons along the outer perimeter are stretched and those along the inner perimeter are compressed, as seen in Fig. 1(a). The out-of-plane strain energy is associated with forming any curved surface of an intrinsically flat material.

In this section, we examine these two contributions to the elastic energy of nanotori. In particular, we will provide and analyze analytical expressions for polyhex nanotori without buckling [29]. For polygonal nanotori, we will show that the contribution from the in-plane strain is negligible, similar to the case of small fullerenes [17].

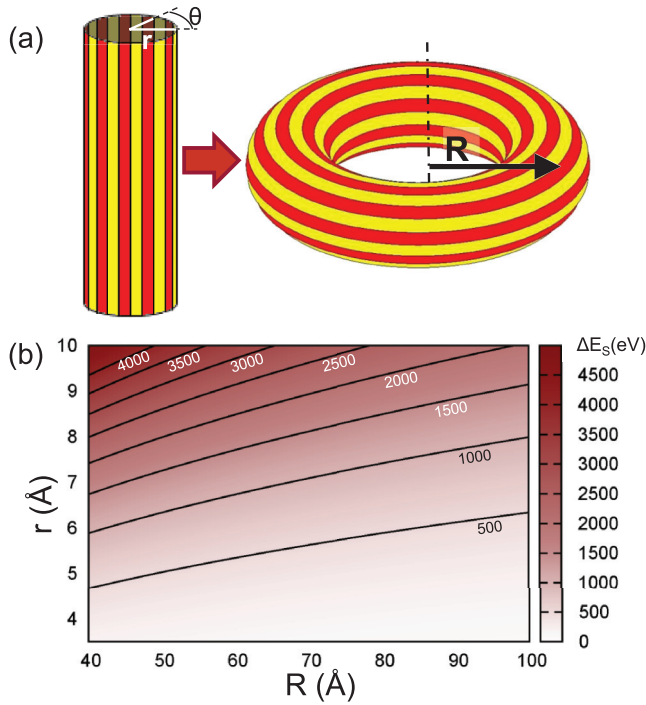


FIG. 2. (Color online) (a) Schematic of a striped nanotube (left), which is bent to a nanotorus (right). (b) Contour plot representing the in-plane strain energy  $\Delta E_s(R, r)$  according to Eq. (9).

### A. In-plane strain energy in polyhex nanotori

Points on the surface of a perfect parametric torus are described by

$$\begin{aligned} x &= (R - r \cos \theta) \cos \phi, \\ y &= (R - r \cos \theta) \sin \phi, \\ z &= r \sin \theta. \end{aligned} \quad (5)$$

Here and in Fig. 1(c),  $R$  is the major and  $r$  is the minor radius,  $\theta$  is the zenith angle, and  $\phi$  is the azimuthal angle. Note that  $R > r$  is required for a normal ring torus without self-intersection. A polyhex nanotorus, shown in Fig. 1(a), can be constructed by rolling up a finite CNT and connecting the two ends together, as indicated in Fig. 2(a). The major radius  $R$  of the polyhex nanotorus can be approximated by the length of the original nanotube divided by  $2\pi$ . In this case, the area density of atoms is smaller than the average along the outer perimeter of the torus, characterized by  $\pi/2 < \theta < 3\pi/2$ , and larger along the inner perimeter. Obviously, the in-plane strain will be negligible in comparison to the out-of-plane strain if  $R \gg r$ . Should this not be the case, then the in-plane strain energy will be important, as it describes the significant distortion of hexagonal rings along the inner and the outer perimeters of a polyhex nanotorus, which are highlighted in Fig. 1(a).

Here we present a simple estimation of the in-plane strain energy for polyhex nanotori without buckling. As shown in Fig. 2(a), a CNT can be seen as parallel narrow strips or nanoribbons of equal length  $2\pi R$  that are connected side by side. After the CNT is deformed to a nanotorus, the strips on the inside of the nanotorus are compressed and the strips on the

outside are stretched. We further assume that the contributions from all other in-plane distortion modes are negligible. As shown in Fig. 2(a), the width of the strips is  $r d\theta$  and the length is  $2\pi(R - r \cos \theta)$ . The strain  $\sigma$  of the strips can be written as

$$\sigma(\theta) = \frac{2\pi(R - r \cos \theta) - 2\pi R}{2\pi R} = -\frac{r}{R} \cos \theta. \quad (6)$$

The total in-plane strain energy of the nanotorus is just the sum of the strain energies of all the strips,

$$\Delta E_s = \int_0^{2\pi} \epsilon(\sigma) 2\pi(R - r \cos \theta) r d\theta. \quad (7)$$

Here,  $\epsilon(\sigma)$  is the energy cost per area of graphene subject to uniaxial strain  $\sigma$ . For sufficiently small strain ( $\sigma \lesssim 5\%$ ),  $\epsilon(\sigma)$  is a parabolic function of  $\sigma$ ,

$$\epsilon(\sigma) = c\sigma(\theta)^2 = c \frac{r^2}{R^2} \cos^2 \theta. \quad (8)$$

Substituting Eq. (8) into Eq. (7), we obtain an expression for the total in-plane strain energy of a nanotorus:

$$\begin{aligned} \Delta E_s &= \int_0^{2\pi} c \frac{r^2}{R^2} \cos^2 \theta 2\pi(R - r \cos \theta) r d\theta \\ &= 2\pi^2 c \frac{r^3}{R}. \end{aligned} \quad (9)$$

The behavior of  $\Delta E_s(R, r)$  in polyhex nanotori is shown in Fig. 2(b). The numerical values in this and following figures for these graphitic carbon nanostructures are based on fits to DFT calculations of graphene. These DFT calculations yield the numerical value  $c = 9.94 \text{ eV/\AA}^2$  and the elastic constants [17]  $D = 1.41 \text{ eV}$  and  $\alpha = 0.165$ , which agree well with values obtained by other theoretical calculations [30–32] and experimental data [33].

As suggested by Eq. (9), the strain energy is proportional to  $r^3$  and inversely proportional to  $R$ . Note that this expression is obtained in the harmonic limit of small strain, which translates into  $R \gg r$ . Also, we have assumed that the nanotori are ideal and described by Eq. (5). In reality, the cross-section of an elastic nanotorus may deviate from a perfect circle upon relaxation, and buckling may occur along the perimeter. In spite of its limits, this expression provides a concrete estimate of the strain energy of experimentally observed rings based on CNTs [34–38]. In the reported cases,  $R$  is of the order of microns and  $r$  of the order of nanometers, so all assumptions in deriving Eq. (9) are justified.

### B. Out-of-plane strain energy in a perfect parametric torus

Besides the in-plane strain, there is also an out-of-plane strain caused by deviation from planarity, which is represented by Eq. (1). For the parametric torus given in Eq. (5), we infer the infinitesimal area  $dA$  in Eq. (1) to be  $dA = r d\theta \cdot (R - r \cos \theta) d\phi$ . Obviously,  $r$  is one of the principal radii of curvature, which is arbitrarily chosen to be  $R_1$ . The situation is more complicated for  $R_2$ , the other principal radius of curvature. As illustrated in Fig. 3,  $R_2$  is given by

$$R_2(\theta) = \begin{cases} R \sec \theta - r & \text{for } -\frac{\pi}{2} < \theta < \frac{\pi}{2} \\ r - R \sec \theta & \text{for } +\frac{\pi}{2} < \theta < \frac{3\pi}{2} \end{cases}. \quad (10)$$

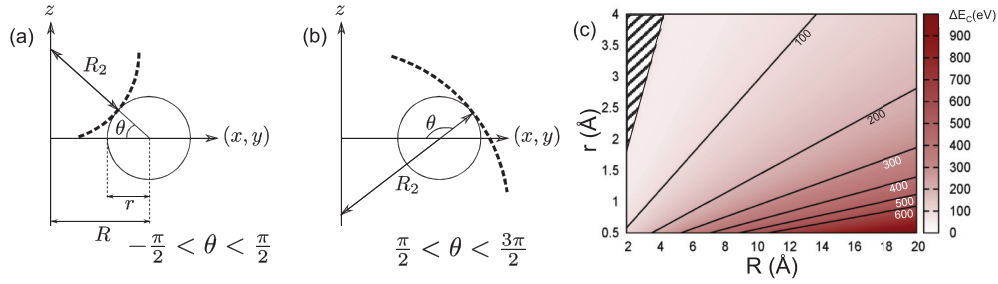


FIG. 3. (Color online) Definition of the principal radius  $R_2$  of a nanotorus in (a) its interior and (b) its exterior part as a function of the zenith angle  $\theta$ . (c) Contour plot displaying the out-of-plane curvature energy  $\Delta E_c(R, r)$  of nanotori according to Eq. (11).

Clearly,  $R_2 \rightarrow \infty$  when  $\theta = \pm \frac{\pi}{2}$ , which is indeed the case since the torus is tangent to the planes  $z = \pm r$ .

Now the evaluation of  $\Delta E_c$  according to Eq. (1) is straightforward. Since the integrand is independent of  $\phi$ , we end up with the expression

$$\begin{aligned} \Delta E_c(R, r) &= \pi D r \int_0^{2\pi} d\theta (R - r \cos \theta) \\ &\quad \times \left( \frac{1}{R_1^2} + \frac{1}{R_2(\theta)^2} + \frac{2\alpha}{R_1 R_2(\theta)} \right) \\ &= 2\pi^2 D \frac{R^2}{r \sqrt{(R+r)(R-r)}}. \end{aligned} \quad (11)$$

In contrast to perfectly spherical fullerenes, where  $\Delta E_c$  is trivially independent of the radius [17], the curvature energy for nanotori depends both on the major radius  $R$  and the minor radius  $r$ . The out-of-plane curvature energy  $\Delta E_c(R, r)$  of carbon nanotori is presented in Fig. 3(c).

We find that the curvature energy does not depend on the Poisson ratio  $\alpha$ , a result from the Gauss-Bonnet theorem, which states the Gaussian curvature integrated over a closed surface equals the Euler characteristic ( $\chi$ ) of the surface times  $2\pi$ . Since  $\chi = 0$  for nanotori or other tubular structures,  $\Delta E_c$  does not depend on  $\alpha$ . Note that the  $1/\sqrt{R-r}$  term in the expression diverges at  $R = r$ , corresponding to a horn torus, and becomes imaginary for  $R < r$ , representing spindle nanotori with self-intersection in the center. In addition, taking the limit of  $R \rightarrow \infty$ , this expression reduces to the curvature energy of a straight cylinder of length  $l = 2\pi R$ ,

$$\Delta E_c = \frac{\pi D l}{r}. \quad (12)$$

Also, by setting the derivative of  $\Delta E_c$  with respect to  $R$  to zero, one obtains the minimal torus curvature energy of  $\Delta \bar{E}_c = 4\pi^2 D$  for  $R = \sqrt{2}r$ , as also reported previously [39,40].

As mentioned before, for polyhex nanotori described by Eq. (5) and  $R \gg r$ , the in-plane strain energy can be adequately quantified by Eq. (9) and the out-of-plane strain energy by Eq. (12). Taking polyhex nanotori constructed from (10,10) CNTs with  $r = 7 \text{ \AA}$  as an example, the constraint on the major radius  $R$  for the harmonic approximation in Eq. (8) to hold is estimated to be  $R \gtrsim 150 \text{ \AA}$ . For  $R = 150 \text{ \AA}$  we find that the in-plane strain energy  $\Delta E_s = 450 \text{ eV}$  and the out-of-plane strain energy  $\Delta E_c = 600 \text{ eV}$  are of the same order. On the other hand, the majority of rings [35,36] synthesized by ultrasonic

wave treatment of CNTs in solution has  $R = 3500 \text{ \AA}$ . In those rings, the contribution from the in-plane strain,  $\Delta E_s = 20 \text{ eV}$ , is negligible in comparison with the out-of-plane strain of  $\Delta E_c = 1.4 \times 10^4 \text{ eV}$ .

### C. Strain energy in polygonal nanotori

In general, the shape of a polygonal nanotorus deviates from that of a perfect parametric torus due to the presence of nonhexagonal defects in a hexagonal network. The largest changes in the curvature occur near individual nonhexagonal defects, and often there are relatively flat segments in-between the defects. Consequently, the analytical expression in Eq. (11) should only be used as a very approximate way to estimate the strain energy of a polygonal nanotorus that is roughly characterized by a set of effective torus radii ( $R, r$ ). For a quantitatively better energy estimate, we must use the discretized version of Eqs. (1) and (2), that takes into account the specific shape of a carbon nanotorus. As mentioned previously, we first obtain the molecular geometry from the classical Keating force field [19].

Once the optimum geometry is established, the local mean curvature  $k_i$  and the local Gaussian curvature  $G_i$  are determined everywhere and substituted into Eq. (2). The results of this methodology to a subset of 22 polygonal nanotori are shown in Fig. 4(a). Here, the strain energy calculated through Eq. (2) with geometry optimized by the Keating potential is represented by the green squares, the energy calculated with the accurate DFT method by black dots, and the Keating potential energy for the Keating-optimized geometry by red rhombi. Our results show clearly that for Keating-optimized geometries, strain energies based on Eq. (2) reproduce our *ab initio* results rather well. On the other side, strain energies estimated using Keating potential alone not only significantly underestimates the strain, but also do not follow the correct general trend. This firmly establishes the applicability of the continuum methodology to polygonal nanotori under investigation.

For specific nanotori, local geometric features that are not described by Eq. (5) contribute to strain energy in addition to Eq. (11). Corresponding results are presented in Fig. 4(b). We considered a large set of polygonal nanotori, which were optimized by the Keating potential, and fitted a pair of torus radii ( $R, r$ ) for each of them. We then correlated the strain energy  $\Delta E_c^A$  obtained using the analytical expression in Eq. (11) with the more proper value  $\Delta E_c^{\text{Keating}}$  based on

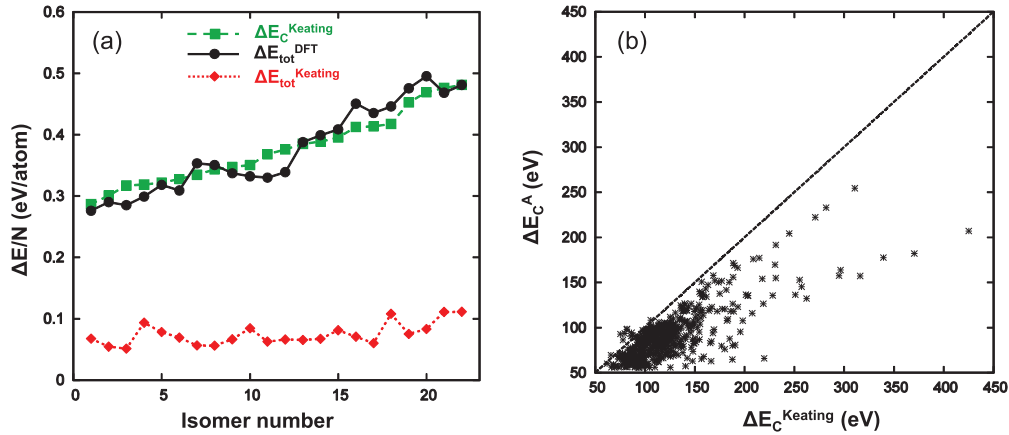


FIG. 4. (Color online) Strain energy  $\Delta E$  in different polygonal nanotori. (a) Energy differences per atom  $\Delta E_{\text{tot}}^{\text{DFT}}$  based on DFT and  $\Delta E_{\text{tot}}^{\text{Keating}}$  based on the Keating potential are presented next to curvature energies  $\Delta E_c^{\text{Keating}}$  based on Eq. (2) for Keating-optimized geometries, described in more detail in the text. (b) Comparison between the analytical expression in Eq. (11) for the curvature energy  $\Delta E_c^A$  based on the elastic description of a parametric torus and the curvature energy  $\Delta E_c^{\text{Keating}}$  obtained using Eq. (2) for Keating-optimized discrete torus geometries.

the optimum discrete geometry and Eq. (2). As expected, most data points lie below the dashed  $\Delta E_c^A = \Delta E_c^{\text{Keating}}$  line. Even though the strain energies estimated using the two approaches appear proportional to each other, it is clear that the analytical expression in Eq. (11) underestimates strain in polygonal nanotori significantly. We conclude that while a quick estimate of the strain energy based on Eq. (11) is useful once the global parameters ( $R, r$ ) are known, Eq. (2) should be used if quantitative comparison among different structures is intended.

## V. LOCAL STABILITY ANALYSIS OF POLYGONAL NANOTORI

In the previous section, we have considered nanotori as whole objects and established elasticity theory as a valid tool to estimate strain energy with respect to planar graphene in different torus isomers. The total strain energy  $\Delta E$ , according to Eqs. (1)–(3), may be represented as an integral or a sum of local contributions. In other words, unlike in more complex DFT calculations, this approach allows to estimate local contributions towards the total strain energy. In the following, we will investigate the local strain distributions within individual nanotori. Next, we will apply this approach to analyze three series of polygonal nanotori and discuss trends in the strain energy in the light of a corresponding asymptotic analysis.

### A. Local curvature distribution

The local geometry of a smooth, two-dimensional object may be characterized by two independent quantities, such as the local mean curvature  $k$  and the local Gaussian curvature  $G$ . These quantities can be used in Eq. (1) or its discretized counterpart, Eq. (2), to determine the curvature energy. The distribution of the local Gaussian curvature  $G_i$  and the local curvature energy per area,  $\Delta E_c^{(i)}/A_0 = D[2k_i^2 - (1 - \alpha)G_i]$ , across the surface of two representative nanotori is shown in Fig. 5.

In both cases, and others shown in the Appendix, the positively curved segments, shown in red in the left panels, are concentrated near the loci of pentagons along the outer perimeter. The negatively curved segments, shown in blue, are concentrated near the loci of heptagons along the inner perimeter. Specifically, the heptagons along the inner perimeter of the  $C_{320}$  nanotorus in Fig. 5(a) are well separated from the pentagons along the outer perimeter. This is different from the axially elongated  $C_{280}$  torus of Fig. 5(b), where pentagon-heptagon pairs at the upper and lower planes form an azulene-like pattern. As a consequence, the Gaussian curvature is more evenly distributed in the latter. We emphasize again that for closed nanotori, the summation of the local Gaussian curvatures is strictly zero as dictated by the Gauss-Bonnet theorem.

The distribution of the local curvature energy is even more intriguing. Within many nanotori, we investigated, some of

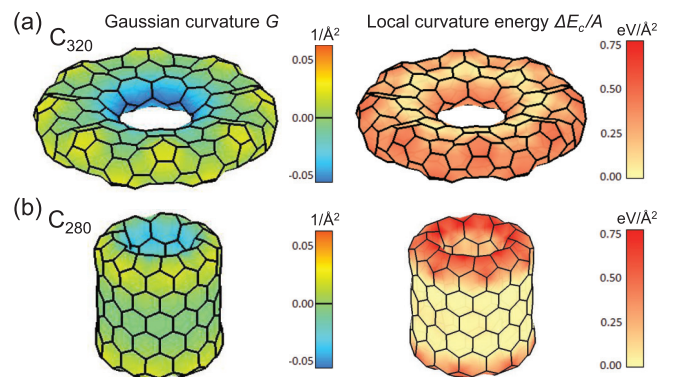


FIG. 5. (Color online) Local Gaussian curvature  $G$  (left panels) and local curvature energy  $\Delta E_c/A$  (right panels) across the surface of selected nanotori. Representative examples shown are (a) the flattened  $C_{320}$  nanotorus with 320 atoms and (b) the elongated  $C_{280}$  nanotorus with 280 atoms.  $G$  and  $\Delta E_c/A$  are interpolated from their values at the atomic sites.

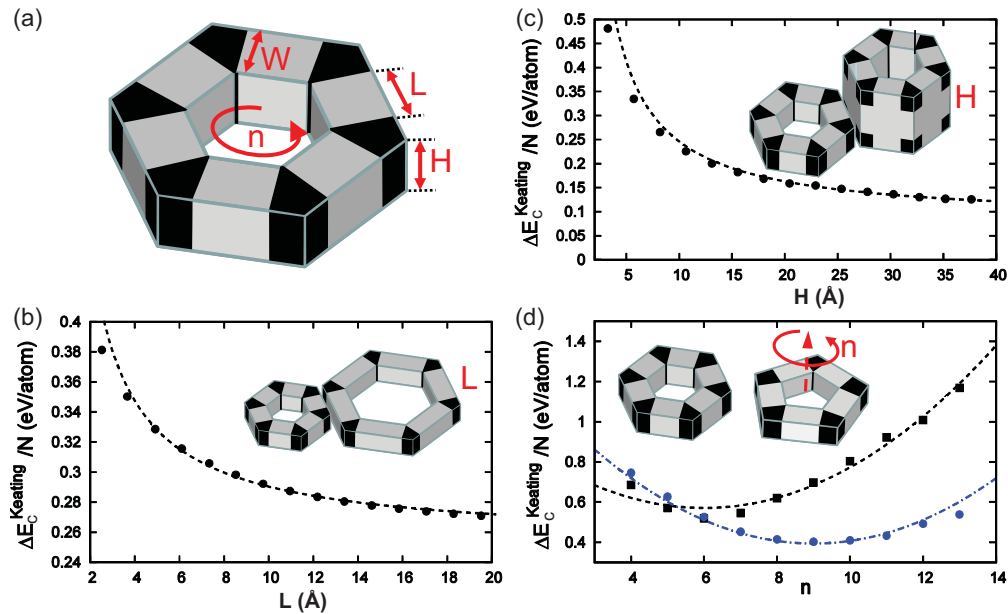


FIG. 6. (Color online) (a) A schematic model of a polygonal nanotorus with  $n$ -fold symmetry ( $n = 6$  is shown here), consisting of  $n$  nanotube segments that are connected by  $n$  nanotube elbow joints. The nanotube segments are characterized by the width  $W$ , length  $L$ , and height  $H$ . (b)–(d) Curvature energies per atom based on Eq. (2) for Keating-optimized nanotori of different shapes.  $\Delta E_c$  is presented for nanotori with (b)  $n, W, H = \text{const.}$ , but nanotube length  $L$  changing, (c)  $n, L, W = \text{const.}$ , but nanotube height  $H$  changing, and (d)  $L, W, H = \text{const.}$ , but rotational symmetry number  $n$  changing. The insets show nanotorus models with different values of  $L$ ,  $H$  and  $n$ . The lines in (b) and (c) are analytical extrapolations discussed in the text. Two sets of data points in (d), connected by lines to guide the eye, correspond to two structural families of nanotori, described in the text.

which are discussed in the Appendix, we observed some degree of correlation between the absolute value of the local Gaussian curvature and the curvature energy. This should imply, at least for the nanotori investigated, that the two local curvatures  $k_i$  and  $G_i$  are not entirely independent. Yet the worth of this correlation has its limitations, as shown in Fig. 5. Whereas in the flattened  $C_{320}$  nanotorus in Fig. 5(a), the curvature energy is rather evenly distributed across the structure, the strain is clearly largest near the upper and lower ends of the  $C_{280}$  nanotorus in Fig. 5(b). This curvature energy distribution in the right panels differs obviously from the Gaussian curvature distribution in the left panels. The reason for this finding is that in these extreme structures, we can not truly decouple  $k_i$  and  $G_i$ . In  $C_{280}$ ,  $G_i \approx 0$  and  $k_i$  is constant in the central “tubular segments.” Only at the upper and lower ends, a large mean curvature  $k_i$  is required to connect the inner and the outer tube. The flatter  $C_{320}$  nanotorus lacks “tubular segments” with  $G_i \approx 0$ . Therefore the Gaussian curvature and curvature energy are better correlated and more evenly distributed in this isomer. The different shapes of carbon nanotori will be discussed in more detail later on.

We need to point out that the determination of the local Gaussian curvature  $G_i$  and the local mean curvature  $k_i$  is a nontrivial task that requires extra attention in discrete, irregular structures. According to the procedure outlined in Ref. [17], the determination of  $G_i$  requires second-nearest-neighbor information. On the other hand, the trivalency of graphitic carbon system lends itself to a compact definition of  $k_i$  based on nearest neighbors only. The asymmetry in handling the two curvatures leads to the possibility of negative local curvature

energies according to Eq. (2), which is unphysical. This can be resolved by lowering the resolution of  $k_i$ , e.g., averaging its values using a window that also includes second-nearest neighbors.

## B. Shape dependence of stability

In spite of a large number of published reports [39–49], a systematic investigation of how the nanotorus stability depends on its shape has been missing. Here we intend to cover this gap by examining the dependence of the total curvature energy on main parameters defining the shape of polygonal carbon nanotori, namely, the rotational symmetry number  $n$ , the length  $L$  and the width  $W$  of the nanotorus segments, and the height  $H$  of the nanotorus, shown schematically in Fig. 6(a). A more detailed classification scheme of polygonal nanotori is provided in Refs. [28,50]. In the following, we discuss the dependence of the curvature energy per atom  $\Delta E_c/N$  on the shape parameters. The structures used to obtain the numerical results in Figs. 6(b)–6(d) are displayed in Figs. 7, 8, and 9, along with the distribution of the local Gaussian curvature and curvature energy following the convention used in Fig. 5.

### 1. Side length dependence

We first look at an interesting case of a polygonal nanotorus consisting of  $n$  straight nanotube segments of finite length  $L$  that are connected by  $n$  elbow joints as illustrated in Fig. 6(a). As suggested in the insets of Fig. 6(b), increasing the length of the nanotube segments reduces gradually the influence of the joints and for large  $L$ , the energy of the elbow joints becomes negligibly small when compared to the curvature energy of the

straight tubular segments. This is illustrated for a specific family of nanotori in Fig. 6(b), where the data points represent results obtained using Eq. (2) for a set of Keating-optimized nanotori with different side length  $L$  that are displayed in the Fig. 7.

For this particular series of nanotori, we may express the curvature energy per atom by  $\Delta E_c(L)/N = a + b/L$  and display this dependence, with  $a = 0.254$  eV and  $b = 0.357$  eV·Å, by the dashed line in Fig. 6(b).

A more specific expression can be derived assuming that the nanotube segments are characterized by the chiral index  $(m, n)$ . In that case, the nanotube radius  $r = 1.42 \text{ Å} \times \sqrt{m^2 + mn + n^2} \times \sqrt{3}/(2\pi)$  can be used in Eq. (12). For a nanotube segment of length  $L$ , the number of atoms can be estimated using  $N = 2\pi r L/A_0$ , where  $A_0 = (1.42 \text{ Å})^2 \times 3\sqrt{3}/4 = 2.62 \text{ Å}^2$  is the area per atom in graphene. Then, we obtain

$$\frac{\Delta E_c(m, n)}{N} = A_0 \frac{\Delta E_c}{2\pi r L} = \frac{\sqrt{3}\pi^2 D}{2(m^2 + mn + n^2)}. \quad (13)$$

The nanotori in Fig. 6(b) are based on (4,4) CNTs, yielding  $\Delta E_c/N = 0.251$  eV, in very good agreement with the fitted constant  $a$ . The residual energy term  $b$  represents the local contribution from the elbow joints, which becomes negligibly small in the large  $L$  limit.

### 2. Height dependence

Next, we study a series of polygonal nanotori resembling double-walled CNTs with their adjacent wall ends connected by a lip-lip interaction [4] in the form of a graphitic network, shown in Fig. 6(c). With increasing height  $H$  of the nanotorus, the curvature energy per atom  $\Delta E_c/N$  will be increasingly dominated by the central tubular part. In analogy to arguments used for nanotori with varying  $L$ , the total number of atoms  $N$  is proportional to  $H$  except a finite number at the double-wall nanotube ends. Then, the curvature energy per atom can be expressed by  $\Delta E_c(H)/N = a' + b'/H$ . This behavior, with the values  $a' = 0.080$  eV and  $b' = 1.658$  eV·Å, is reproduced by the dashed line in Fig. 6(c) for a particular series of nanotori depicted in Fig. 8.

Similar to the case discussed in Fig. 6(b),  $\Delta E_c/N$  can be approximated by the sum of curvature energies of two nanotubes of length  $H$ , the inner one with radius  $r_i$  and the outer one with radius  $r_o$ . Then,

$$\begin{aligned} \frac{\Delta E_c(r_i, r_o)}{N} &= A_0 \frac{\Delta E_c(r_i) + \Delta E_c(r_o)}{2\pi(r_i + r_o)H} = \frac{A_0 D}{2r_i r_o} \\ &= \frac{\sqrt{3}\pi^2 D}{2\sqrt{(m_i^2 + m_i n_i + n_i^2)(m_o^2 + m_o n_o + n_o^2)}}. \end{aligned} \quad (14)$$

For the nanotori presented in Fig. 6(c), the chiral indices are  $(m_i, n_i) = (5, 5)$  and  $(m_o, n_o) = (10, 10)$ , which gives the value  $\Delta E_c/N = 0.080$  eV. This value, again, is in perfect agreement with the fitted value  $a'$  above. Again, the constant  $b'$  term describes the residual energy of the end joints connecting the inner and the outer tube.

In the above energy estimate, we have ignored the interlayer interaction between the outer and inner wall. If the separation

$r_o - r_i$  between the walls were as small as in graphite, this stabilizing interaction would reduce the strain energy by  $\approx 0.03$  eV/atom. In reality, a much smaller effect of this interaction is expected, since the strain at the end junctions tends to keep  $r_o - r_i$  large and since the interaction should depend inversely on  $(r_o - r_i)^6$ . In any case, the interwall interaction is negligibly small in comparison to values shown in Fig. 6(c). In other, nontoroidal structures including helically coiled CNTs [51], the significance of the interwall interaction has to be accounted for on a case-by-case basis.

### 3. Rotational symmetry number dependence

To the best of the authors' knowledge, all polygonal carbon nanotori investigated in the literature had rotational symmetry numbers  $n = 5$  or  $6$ . This is largely due to the fact that a nanotorus can be constructed in a cut-and-paste manner from graphene [28,52,53] while preserving its original hexagonal symmetry. Also the majority of nanotori studied here has been constructed using a scheme generating isomers with either  $D_{nd}$  or  $D_{nh}$  point group symmetry. This constraint reduces greatly the number of possible isomers, but provides for an easy way to characterize individual polygonal nanotori by the relative positions of nonhexagonal rings within a rotational unit cell. With only selected results for  $n = 5$  and  $6$  at hand, no conclusions are possible regarding the dependence of the stability on the rotational symmetry number.

Such results are presented in Fig. 6(d), where we display the curvature energy as a function of the rotational symmetry number, with  $n$  changing from  $n = 4$  to  $13$ , while all other shape parameters are fixed. We focus on two structural nanotori families. The first family, represented by black squares in Fig. 6(d), was studied more extensively in the literature [13,15,39,40] and is found to be most stable for  $n = 6$ . The second family, represented by the blue dots, consists of a series of nanotori with a different distribution of nonhexagonal rings and is energetically optimal for  $n = 9$  instead.

The specific shapes of these two families are presented in Fig. 9. The first family, depicted in the left panels of Fig. 9, has its heptagonal rings clustered in the center of the tori and the pentagonal rings forming one rim at the outer equator. In the second family, depicted in the right panels of Fig. 9, the heptagons are fully separated inside the torus and the pentagons form two groups located at the top and the bottom of the outer rims. In wide tori, the separation between nonhexagonal rings is large and the bends induced by each pentagon-heptagon pair are independent. This is not the case in the narrow tori discussed here, where the separation between nonhexagonal rings is small, causing elastic coupling between adjacent bends and resulting in a deviation from the presumed sixfold rotational symmetry.

As mentioned above, we find that a significant fraction of the nanotori investigated in this study minimized the curvature energy per atom for other than a sixfold rotational symmetry. As a matter of fact, the distribution of optimum rotational symmetry numbers  $n_{\text{opt}}$ , displayed in Fig. 10(b), is roughly a Gaussian centered at  $n_{\text{opt}} \approx 7$ , with some extreme outliers at  $n_{\text{opt}} = 12$ . We found that the deviation of  $n_{\text{opt}}$  from the expected value  $n_{\text{opt}} = 6$  is an artifact caused by the

parametrized Keating force field, which is penalizing bond length deviations from 1.42 Å more than bond angle deviations from 120°, while underestimating the penalty for out-of-plane bending and thus somewhat distorting the optimum geometry.

The optimality of the  $n = 6$  rotational symmetry number can be restored in the large-torus limit as follows. Let us consider a cut-and-paste model of a graphitic torus with  $n = 6$  in the shape displayed in Fig. 6(a). It is clear that all nonhexagonal rings, which determine the angle  $\varphi = 120^\circ$  between adjacent nanotube segments, will be located in the elbow joints colored in black, whereas the straight grey-colored segments will contain only hexagons. In large tori, the relative role of the elbow joints will play an ever diminishing role, and strain energy will be determined by the shape of the nanotube segments. Deviation from  $n = 6$  will mean that the nanotube segments need to be bent, which causes extra strain.

## VI. CONCLUSIONS

We have presented comprehensive analysis on the elastic energy of carbon nanotori containing either only hexagons (polyhex nanotori) or also other polygons (polygonal nanotori) on the basis of continuum elasticity theory. In polyhex nanotori, we found that depending on the ratio between the major radius  $R$  and minor radius  $r$  of the torus, the in-plane and the out-of-plane contributions to the total elastic energy vary significantly. The wide CNT rings resembling nanotori, which have been observed experimentally, display only negligible in-plane strain, whereas the in-plane strain should exceed the out-of-plane strain for  $R/r \lesssim 20$ . In the polygonal nanotori studied here, the in-plane strain is rather small and the elastic energy obtained with the continuum method is shown to agree quantitatively with the results of *ab initio* DFT calculations. We also show that the analytical expression Eq. (11) can serve as a quick and qualitative reference for the elastic energy of nanotori once the shape parameters ( $R, r$ ) are known.

The capability of the current methodology is further demonstrated by a detailed analysis of the distributions of local excess energy in individual nanotori. Depending on the relative loci of nonhexagonal rings, the distribution of Gaussian curvature, mean curvature, and the local curvature energy can be either localized or evenly distributed across the nanotorus surface. This analysis can be extended to other 2D systems with different chemical composition and shape, and can also be related to the local stability and chemical reactivity index of different sites [17,54].

We have furthermore studied three different sets of polygonal nanotori with varying shape parameters, including the lateral and the axial dimension of the nanotori and the rotational symmetry number. Contrary to the common perception that the most stable nanotori all have a sixfold symmetry, we find that in smaller polygonal nanotori, the optimal rotational symmetry number covers a wide range  $4 \lesssim n_{\text{opt}} \lesssim 12$ . Only in the large-size limit, when the number of nonhexagonal defects is fixed,  $n = 6$  emerges as the optimum rotational symmetry number. Asymptotic analysis on the variation of the other two shape parameters agrees quantitatively with the numerical results. This confirms that the current methodology, at least for the systems investigated here, is applicable across a wide length scale: From small nanotori where *ab initio* calculations

are available, to mesoscopic tori, where continuum elasticity theory applies. Owing to the broad applicability, we believe that our approach will provide valuable results pertaining to the thermodynamical behavior of other large, experimentally observed carbon nanostructures, where atomic-scale treatment by *ab initio* techniques is not practical.

## ACKNOWLEDGMENTS

This work was partly funded by the National Science Foundation Cooperative Agreement No. EEC-0832785, titled “NSEC: Center for High-rate Nanomanufacturing.” Computational resources for this project were provided by the Michigan State University High-Performance Computer Center.

## APPENDIX: NANOTORI WITH DIFFERENT SHAPE PARAMETERS

The global and local curvature energy depends sensitively on the shape parameters of polygonal nanotori. The structure, distribution of local Gaussian curvature  $G$  and local curvature energy  $\Delta E_c/A$  across the surface of all the nanotori presented in Fig. 6 are displayed in Figs. 7–9.

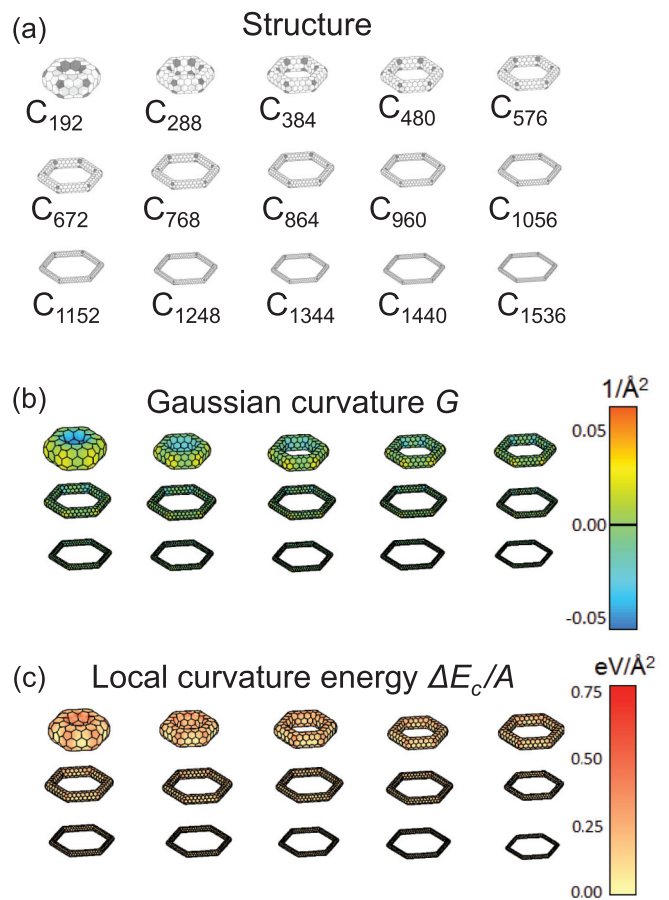


FIG. 7. (Color online) (a) Structural models, (b) local Gaussian curvature  $G$ , and (c) local curvature energy  $\Delta E_c/A$  across the surface of torus isomers with different lengths of the nanotube segments  $L$ , defined in Fig. 6(a). The nonhexagonal rings in (a) are shaded. The values of  $G$  and  $\Delta E_c/A$  have been interpolated from their values at the atomic sites.

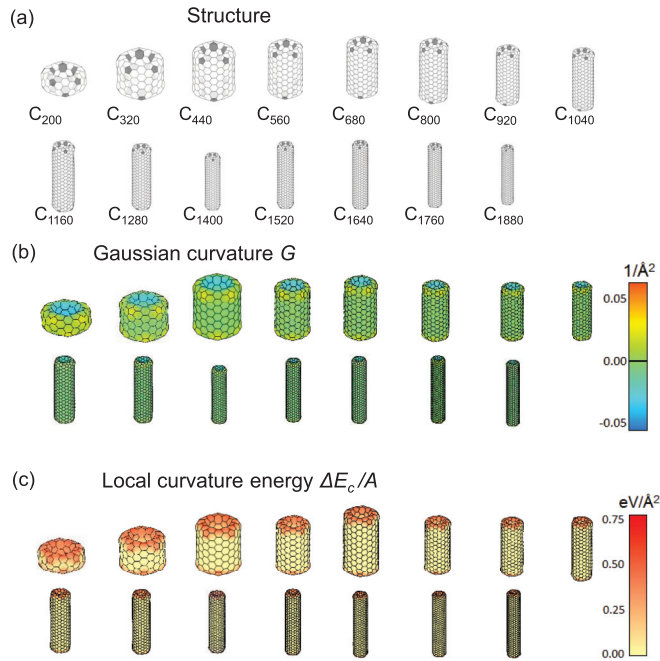


FIG. 8. (Color online) (a) Structural models, (b) local Gaussian curvature  $G$ , and (c) local curvature energy  $\Delta E_c/A$  across the surface of torus isomers with different heights  $H$ , defined in Fig. 6(a). The nonhexagonal rings in (a) are shaded. The values of  $G$  and  $\Delta E_c/A$  have been interpolated from their values at the atomic sites.

### 1. Nanotori with changing side length

In Fig. 7, we present the series of  $D_{6h}$ -symmetric polygonal nanotori with changing length  $L$  of nanotube segments that provided the data points for Fig. 6(b). As is discussed before, a  $D_{nh}$ -symmetric nanotorus can be viewed as  $n$  straight CNT segments connected by  $n$  elbow joints, the loci of nonhexagonal rings. As the side length  $L$  increases, the torus can be asymptotically described by a hexagon of connected nanotubes. On a per-atom basis, the contribution to the excess energy from the elbow joints is negligible in the  $L \rightarrow \infty$  limit. Thus the elastic energy is accounted for simply by the summation of the energy of the six constituent CNTs in this limit.

### 2. Nanotori with changing height

In Fig. 8, we present the series of polygonal nanotori resembling a segment of height  $H$  of a double-walled CNT that provided the data points for Fig. 6(c). The inner and outer tubes are connected at the top and the bottom by lip-lip interactions consisting of hexagonal and nonhexagonal rings. In the  $H \rightarrow \infty$  limit, the elastic energy contribution from the two ends is a constant, and the nanotorus essentially resembles an infinitely long double-walled CNT in terms of stability.

### 3. Nanotori with changing rotational symmetry

In Fig. 9 we present polygonal nanotori with changing rotational symmetry number  $n$  that provided the data points

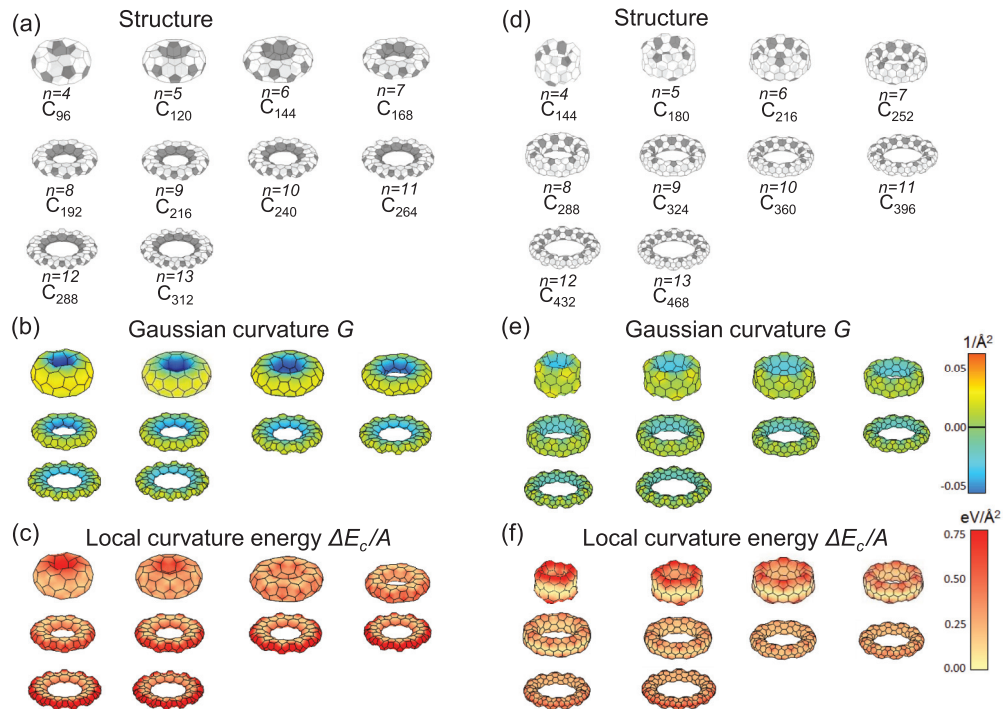


FIG. 9. (Color online) [(a) and (d)] Structural models, [(b) and (e)] local Gaussian curvature  $G$ , and [(c) and (f)] local curvature energy  $\Delta E_c/A$  across the surface of torus isomers with different rotational symmetry numbers  $n$ , defined in Fig. 6(a). Structures in [(a) and (c)] and [(d) and (f)] represent two distinct torus families. The nonhexagonal rings in (a) and (d) are shaded. The values of  $G$  and  $\Delta E_c/A$  have been interpolated from their values at the atomic sites.

for Fig. 6(d). We focus on two families of nanotori and display them in Figs. 9(a)–9(c) and 9(d)–9(f). In each of the two families, the relative positions of the nonhexagonal rings remain the same while the rotational symmetry number  $n$  changes from  $n = 4$  to 13. Depending on the detailed arrangement of the nonhexagonal rings, we find that the local curvature and strain energy distribution changes strongly. Even more important, the dependence of the strain energy on  $n$  is very different for the two families of nanotori, as seen in Fig. 6(d).

The change in the distribution of the local curvature in the two families of nanotori is evident when comparing results in Figs. 9(c) and 9(f) for increasing values of  $n$ . In the first family of nanotori in Fig. 9(c), we observe an abrupt redistribution of the curvature energy from the inner part to the outer part of the torus with increasing  $n$ . As seen in Fig. 9(f), such a transition does not occur in the second family of nanotori. There, the curvature energy is largest at the top and the bottom rims for small values of  $n$  and is gradually redistributed to the outer part for large  $n$  values.

To better examine the stability of nanotori as a function of  $n$ , we selected most stable structures from a huge pool of polygonal nanotori. Our selection criterion was that the heat of formation be less than +0.8 eV/atom based on the AM1 total energy functional [55] and number of atoms per rotational unit cell be at most 40. While AM1 is not as reliable as density

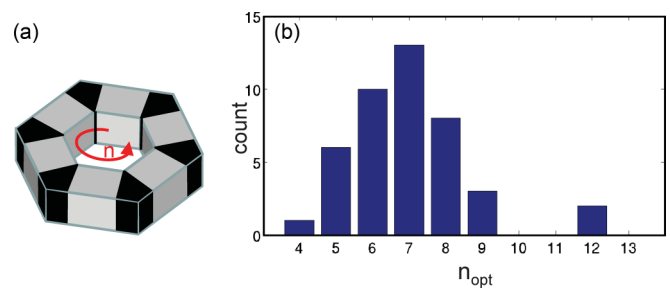


FIG. 10. (Color online) (a) A schematic model of a polygonal nanotorus with an  $n$ -fold ( $n = 6$  in this case) symmetry. (b) Distribution of the optimal rotational symmetry numbers  $n_{opt}$  in the 43 families of polygonal nanotori covered in this study.

functional theory calculations, it provides reasonable energy estimates, including the value of +0.7 eV for the heat of formation of the  $C_{60}$ , somewhat larger than the observed value of +0.4 eV. The above stated selection criterion filtered out 43 nanotori with different distributions of nonhexagonal rings, defining a torus family. For each of the 43 families, we varied the rotational symmetry number  $n$  in the range  $4 \leq n \leq 13$  to find the optimal value of  $n$ . The distribution of the  $n_{opt}$  is shown in Fig. 10(b). As mentioned earlier, the distribution is roughly a Gaussian centered at  $n_{opt} = 7$ , with some surprising outliers at  $n_{opt} = 12$ .

- 
- [1] H. W. Kroto, J. R. Heath, S. C. O'Brien, R. F. Curl, and R. E. Smalley, *Nature (London)* **318**, 162 (1985).
- [2] S. Iijima, *Nature (London)* **354**, 56 (1991).
- [3] K. S. Novoselov, A. K. Geim, S. V. Morozov, D. Jiang, Y. Zhang, S. V. Dubonos, I. V. Grigorieva, and A. A. Firsov, *Science* **306**, 666 (2004).
- [4] D. Tománek, *Guide Through the Nanocarbon Jungle* (IOP Publishing, Bristol, UK, 2014).
- [5] M. S. Dresselhaus, G. Dresselhaus, and P. Avouris, *Carbon Nanotubes: Synthesis, Structure, Properties, and Applications* (Springer, Berlin, 2001).
- [6] L. Liu and J. Zhao, in *Syntheses and Applications of Carbon Nanotubes and Their Composites*, edited by S. Suzuki (InTech, Rijeka, Croatia, 2013).
- [7] M. Zheng and C. Ke, *Small* **6**, 1647 (2010).
- [8] L. Chen, H. Wang, J. Xu, X. Shen, L. Yao, L. Zhu, Z. Zeng, H. Zhang, and H. Chen, *J. Am. Chem. Soc.* **133**, 9654 (2011).
- [9] L. Liu, G. Y. Guo, C. S. Jayanthi, and S. Y. Wu, *Phys. Rev. Lett.* **88**, 217206 (2002).
- [10] M.-F. Lin, *J. Phys. Soc. Jpn.* **67**, 1094 (1998).
- [11] M. F. Lin and D. S. Chuu, *Phys. Rev. B* **57**, 6731 (1998).
- [12] C. G. Rocha, M. Pacheco, Z. Barticevic, and A. Latgé, *Phys. Rev. B* **70**, 233402 (2004).
- [13] A. Ceulemans, L. F. Chibotaru, and P. W. Fowler, *Phys. Rev. Lett.* **80**, 1861 (1998).
- [14] T. A. Hilder and J. M. Hill, *Phys. Rev. B* **75**, 125415 (2007).
- [15] M. T. Lusk and N. Hamm, *Phys. Rev. B* **76**, 125422 (2007).
- [16] N. Hamada, S.-i. Sawada, and A. Oshiyama, *Phys. Rev. Lett.* **68**, 1579 (1992).
- [17] J. Guan, Z. Jin, Z. Zhu, C. Chuang, B.-Y. Jin, and D. Tománek, *Phys. Rev. B* **90**, 245403 (2014).
- [18] L. D. Landau, L. P. Pitaevskii, A. M. Kosevich, and E. M. Lifshitz, *Theory of Elasticity*, Course of Theoretical Physics, 3rd ed. (Pergamon Press, London, England, 1959), Vol. 7.
- [19] P. N. Keating, *Phys. Rev.* **145**, 637 (1966).
- [20] E. Artacho, E. Anglada, O. Dieguez, J. D. Gale, A. Garcia, J. Junquera, R. M. Martin, P. Ordejon, J. M. Pruneda, D. Sanchez-Portal, and J. M. Soler, *J. Phys.: Condens. Matter* **20**, 064208 (2008).
- [21] D. M. Ceperley and B. J. Alder, *Phys. Rev. Lett.* **45**, 566 (1980).
- [22] J. P. Perdew and A. Zunger, *Phys. Rev. B* **23**, 5048 (1981).
- [23] N. Troullier and J. L. Martins, *Phys. Rev. B* **43**, 1993 (1991).
- [24] H. J. Monkhorst and J. D. Pack, *Phys. Rev. B* **13**, 5188 (1976).
- [25] M. R. Hestenes and E. Stiefel, *J. Res. Natl. Bur. Stand.* **49**, 409 (1952).
- [26] G. Overney, W. Zhong, and D. Tomanek, *Z. Phys. D* **27**, 93 (1993).
- [27] C. Q. Ru, *Phys. Rev. B* **62**, 9973 (2000).
- [28] C. Chuang, Y.-C. Fan, and B.-Y. Jin, *J. Chem. Inf. Model.* **49**, 361 (2009).
- [29] O. Hod, E. Rabani, and R. Baer, *Phys. Rev. B* **67**, 195408 (2003).
- [30] K. N. Kudin, G. E. Scuseria, and B. I. Yakobson, *Phys. Rev. B* **64**, 235406 (2001).
- [31] P. Koskinen and O. O. Kit, *Phys. Rev. B* **82**, 235420 (2010).
- [32] R. Faccio, P. A. Denis, H. Pardo, C. Goyenola, and Álvaro W. Mombrú, *J. Phys.: Condens. Matter* **21**, 285304 (2009).
- [33] R. Nicklow, N. Wakabayashi, and H. G. Smith, *Phys. Rev. B* **5**, 4951 (1972).

- [34] M. Ahlskog, E. Seynaeve, R. Vullers, C. Van Haesendonck, A. Fonseca, K. Hernadi, and J. B Nagy, *Chem. Phys. Lett.* **300**, 202 (1999).
- [35] R. Martel, H. R. Shea, and P. Avouris, *J. Phys. Chem. B* **103**, 7551 (1999).
- [36] R. Martel, H. R. Shea, and P. Avouris, *Nature (London)* **398**, 299 (1999).
- [37] L. Song, L. J. Ci, L. F. Sun, C. Jin, L. Liu, W. Ma, D. Liu, X. Zhao, S. Luo, Z. Zhang, Y. Xiang, J. Zhou, W. Zhou, Y. Ding, Z. L. Wang, and S. Xie, *Adv. Mater.* **18**, 1817 (2006).
- [38] C. R. Chang, L. H. Lu, J. H. Liu, and W. Chen, *Chem. Phys.* **393**, 123 (2012).
- [39] J. E. Avron and J. Berger, *Phys. Rev. A* **51**, 1146 (1995).
- [40] J. Berger and J. E. Avron, *J. Chem. Soc., Faraday Trans.* **91**, 4037 (1995).
- [41] B. I. Dunlap, *Phys. Rev. B* **50**, 8134 (1994).
- [42] B. I. Dunlap, *Phys. Rev. B* **46**, 1933 (1992).
- [43] S. Itoh, S. Ihara, and J.-I. Kitakami, *Phys. Rev. B* **47**, 1703 (1993).
- [44] S. Ihara, S. Itoh, and J.-I. Kitakami, *Phys. Rev. B* **47**, 12908 (1993).
- [45] S. Itoh and S. Ihara, *Phys. Rev. B* **48**, 8323 (1993).
- [46] S. Itoh and S. Ihara, *Phys. Rev. B* **49**, 13970 (1994).
- [47] S. Ihara, S. Itoh, K. Akagi, R. Tamura, and M. Tsukada, *Phys. Rev. B* **54**, 14713 (1996).
- [48] R. Setton and N. Setton, *Carbon* **35**, 497 (1997).
- [49] I. László and A. Rassat, *J. Chem. Inf. Comput. Sci.* **43**, 519 (2003).
- [50] C. Chuang, Y.-C. Fan, and B.-Y. Jin, *J. Chem. Inf. Model.* **49**, 1679 (2009).
- [51] C. Chuang, Y.-C. Fan, and B.-Y. Jin, *J. Mol. Struct.* **1008**, 1 (2012).
- [52] R. Tamura, M. Ikuta, T. Hirahara, and M. Tsukada, *Phys. Rev. B* **71**, 045418 (2005).
- [53] F. Beuerle, C. Herrmann, A. C. Whalley, C. Valente, A. Gamburd, M. A. Ratner, and J. F. Stoddart, *Chem. Eur. J.* **17**, 3868 (2011).
- [54] A. A. Pacheco Sanjuan, M. Mehboudi, E. O. Harriss, H. Terrones, and S. Barraza-Lopez, *ACS Nano* **8**, 1136 (2014).
- [55] M. J. S. Dewar, E. G. Zoebisch, E. F. Healy, and J. J. P. Stewart, *J. Am. Chem. Soc.* **107**, 3902 (1985).